Resonant Josephson tunneling in S-I-S′-I-S multilayered devices

I. P. Nevirkovets*
Department of Physics and Astronomy, Northwestern University, 2145 Sheridan Road, Evanston, Illinois 60208

S. E. Shafranjuk†
Research Institute of Electrical Communication, Tohoku University, 2-1-1, Katahira, Aoba-ku, Sendai 980, Japan
(Received 10 March 1998; revised manuscript received 13 July 1998)

It was observed experimentally that the magnitude of the Josephson current through a single junction in the double-barrier Nb/Al-AlO_x-Nb/Al-AlO_x-Nb stack is lower than that for the whole device. This effect is explained by a model that takes into account Andreev reflection in the S-I-S′-I-S double-barrier stack, where S and S′ are superconductors and I is an insulator. The middle S′ layer is very thin (with the thickness of order the coherence length) and has reduced superconducting parameters as compared with the external S layers. The model predicts bound state levels in the middle electrode. The bound states provide an additional channel of Josephson tunneling which results in enhanced Josephson critical current density through the stack as compared with that for the single S-I-S′ junction. [S0163-1829(98)05114-5]

I. INTRODUCTION

The study of superconducting multilayered structures is closely linked to the Josephson effect that is the most fundamental indication of the quantum coherent properties of the superfluid condensate. Even the simplest junctions like those consisting of two superconducting electrodes, S, separated by an insulator, I, (the weak coupled S-I-S junction), or by a normal metal, N, (the strong coupled S-N-S junction), show remarkable features. For instance, the multiple Andreev reflection[1] at the S-N and N-S interfaces may result in subharmonic energy-gap structure in the current-voltage (I-V) characteristic.[2–4] The Andreev bound state (BS) resonance levels positioned in the middle N electrode carry the supercurrent across the S-N-S junction[5–8] (see also Refs. 9–11 and related references there), while the coherent tunneling of Cooper pairs through S-I-S junction depends on the electron spectrum and on the distribution of electron excitations in the electrodes (see, e.g., Refs. 12,13). The combination of both weak and strong Josephson couplings may occur in many complex systems, e.g., in the conventional superconducting multilayers, or in the cuprate single crystals, where BS levels[14] may coexist on the atomic scale with the intrinsic Josephson effect happening between adjacent superconducting Cu-O planes.[15] In that kind of system, one can expect a close relation between the resonance BS and the Josephson tunneling, because physically the BS causes an additional coherence of the electron states, which results in peculiarities in the electron spectrum. Since the tunneling probability is generally proportional to the magnitude of the electron density of states $N(E_n)$ (E_n is the energy eigenvalue with quantum number *n)* in the electrodes, an additional channel of the Josephson tunneling should arise due to the BS contribution. Hence, an enhanced value of the supercurrent may be expected in Josephson systems that poses the Andreev BS.

In this paper, the Josephson current enhancement is studied experimentally and theoretically using the S-I-S′-I-S setup. The middle superconducting electrode S′ has lower critical parameters compared to S, and is supposed to create a quantum well with the Andreev resonance BS levels inside. To distinguish the BS contribution, we compare the Josephson current across the total S-I-S′-I-S setup with the tunneling supercurrent between the adjacent S and S′ electrodes (the S-I-S′ part of the total setup).

Our aim was to study the magnitude of the Josephson current in the double-barrier tunnel junction devices with very thin middle electrodes, where the two junctions are separated by a distance of the order of the coherence length ξ. In this case, we expected to see additional interference effects between the junctions as compared to the commonly considered case when the junctions in the stack are separated by a distance less than the London penetration depth, λ_L, but exceeding ξ.[16,17] We have carried out a comparative study of the Nb/Al-AlO_x-Nb/Al-AlO_x-Nb and Nb/Al-AlO_x-Nb/Al-AlO_x-Ta/Nb devices fabricated in identical configurations from the structures deposited in the same run. The devices were S-I-S′-I-S- and S-I-S′-I-N/S-type, respectively, with the critical temperature, T_c', of the S′ layer being lower than the T_c of the S layers. By analyzing the I-V characteristics of the devices, we concluded that the maximum Josephson current density, J_c, through the S-I-S′-I-S device is higher than the corresponding J_c through the single S′-I-S junction from the stack.

To give a theoretical interpretation of the observed phenomena, we present a theoretical model that examines the BS resonance contribution to the Josephson effect in the case of S-I-S′-I-S devices. We compute the energy spectrum, E_n, and electric current of the multilayered system. In a Josephson system, the supercurrent depends upon the phase shift φ of the condensate wave functions inside the electrodes and may be written in general form as

$$I=\frac{2\pi}{\Phi_0}\sum_n \frac{\partial E_n}{\partial \varphi}(1-f_{E_n}), \tag{1}$$

where f_{E_n} is the electron distribution function, $\Phi_0=h/2e$ is the flux quantum, e is the electron charge, h is the Plank constant. Our calculations show that, compared to the S-I-S

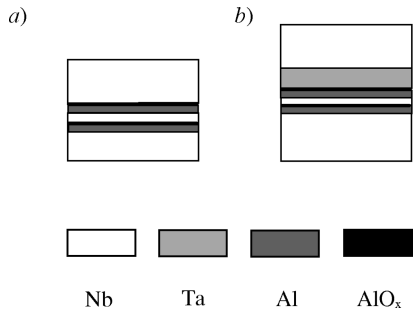

FIG. 1. Schematic cross-sectional view of type-1 (a) and type-2 (b) devices.

case, additional branches of BS may occur in the electronic spectrum of the S-I-S′-I-S system. In particular, we find qualitatively different features, e.g., BS having the shape of ''islands'' being closed between ''turning points,'' φ_1 and φ_2. In those points $\partial E_n(\varphi)/\partial\varphi$ diverges and consequently, the Josephson current may be essentially increased. The resonance due to presence of the BS, and particularly due to ''island'' BS, is suitable to explain the enhanced magnitude of I_c in our experiment.

II. EXPERIMENT

The double-barrier devices were fabricated from Nb/Al-AlO$_x$-Nb/Al-AlO$_x$-Nb (type 1) and Nb/Al-AlO$_x$-Nb/Al-AlO$_x$-Ta/Nb (type 2) structures deposited in the same vacuum run to provide identical material parameters of the films and tunnel barriers. The fabrication procedure is described in more detail in Ref. 18. It is important that we obtained devices identical in all the respects, with the exception of different counterelectrodes. The thickness of the bottom and the topmost Nb electrodes was $d_1=150$ nm and $d_3=130$ nm, respectively, whereas the total thickness of the middle Nb/Al electrode was $d_2=9$ nm. The devices are square-shaped with an in-plane area of 9×9 μm^2. The cross-sectional view of both types of devices is shown schematically in Fig. 1. Both top and bottom junctions had approximately equal specific tunnel resistances of order 10^{-6} $\Omega\times$cm^2. I-V characteristics of the two planar arrays, each consisting of seven identical double-barrier devices of definite type connected in a series, are shown in Fig. 2. Therefore, each array consists of a total of 14 junctions. Curves 1 and 2 are for type 1 and type 2 devices, respectively. At successive voltages, the I-V characteristics reveal a fine step structure that is due to transitions into the resistive state of the single junctions in the array. For the array consisting of the type 1 devices (curve 1), the critical current value averaged over 14 junctions is $I_c=0.80\pm0.04$ mA. In the calculation of this value, we could not distinguish the critical currents of the top and bottom junctions because they were very close to each other.

Now we consider the curve 2 in Fig. 2. It is the sum of the I-V characteristics of Nb/Al-AlO$_x$-Nb/Al and Nb/Al-AlO$_x$-Ta/Nb junctions. The Ta film deposited under the conditions of this experiment was not superconducting at $T=4.2$ K. Thus, the I-V characteristic of the Nb/Al-AlO$_x$-Ta/Nb junction has a shape close to that of S-I-N junction. A small supercurrent through the

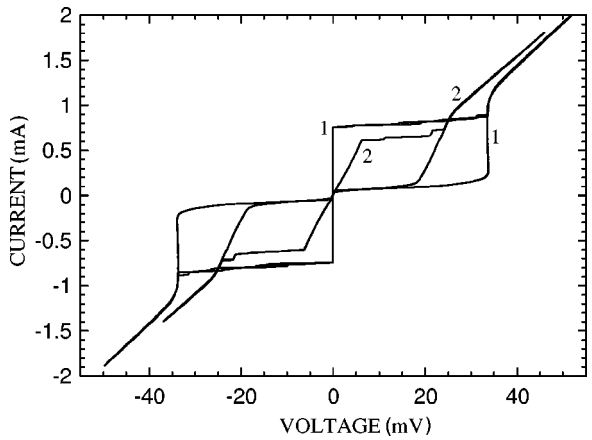

FIG. 2. $I-V$ characteristics of seven identical devices connected in a series. Curve 1 is for Nb/Al-AlO$_x$-Nb/Al-AlO$_x$-Nb and curve 2 is for Nb/Al-AlO$_x$-Nb/Al-AlO$_x$-Ta/Nb devices, respectively.

Nb/Al-AlO$_x$-Ta/Nb junction is due to the proximity effect of Ta with the topmost Nb film.

The bottom Nb/Al-AlO$_x$-Nb/Al junction is an S′-I-S-type junction. In the total I-V characteristic of the considered array, the critical current of the bottom junctions reveals itself as voltage ''jumps'' from the branch corresponding to the top junctions. The average value of the critical current for the seven bottom junctions is $I_c=0.64\pm0.04$ mA. Therefore, the difference in the magnitude of I_c through the bottom junction in type 2 devices and I_c through the two junctions in type 1 devices is about 20%, which exceeds the experimental uncertainty of the I_c measurement. Since the bottom Nb/Al-AlO$_x$-Nb/Al junction in the type 2 devices is identical to the bottom junction in the type 1 devices, this indicates enhancement of the I_c through the S-I-S′-I-S device as compared with the I_c of the single S′-I-S junction in the same stack. In other words, it means that if the superconductivity of an external electrode in the double-junction S-I-S′-I-S stack is deteriorated, then the supercurrent through the neighbor junction is reduced. Our preliminary experimental investigation has shown that this effect is due to physical, rather than technological, origin.[18]

Analysis of the voltage position of gap sum and gap difference features in the I-V characteristics of the devices gives the values $\Delta=1.4$ meV for the bottom and topmost Nb electrodes and $\Delta'=1.0$ meV for the middle Nb/Al layer at $T=4.2$ K. From the temperature dependence of the I-V characteristics, we have determined that the critical temperatures for the respective films are $T_c=8.5$ K and $T_c'=6.2$ K. Therefore, at $T=4.2$ K, there is a considerable difference in the magnitude of the energy gap between the middle superconducting layer and external Nb electrodes for the S-I-S′-I-S device.

The difference in the superconducting parameters between the S and S′ layers is mainly due to the distinct role of the proximity effect. In fact, both of them are Nb/Al proximity ''sandwiches.'' For the relatively thick external S electrodes, the influence of the residual Al layer (which remains after the barrier formation) can be neglected. This is not valid for the very thin middle bilayer; the effect of the Al must be taken into account. Our experiments carried out on similar devices give the value of $\xi\sim10$ nm for thin Nb

layers.[19] Since for the middle S′ layer the thickness of both Nb and Al is less than this value, we will consider it as a uniform superconducting film with the critical parameters cited above.

III. THEORETICAL MODEL

A simple model which we apply in this paper to interpret the obtained experimental results in the symmetric S-I-S′-I-S multilayered Josephson structures is based on the solution of the Bogolubov equation in the rectangular approximation.[20] This approach can be easily extended for arbitrary temperatures[21] and also can include many-body effects.[22] Initially we assume here the ballistic ''clean limit'' (when the electron-impurity elastic scattering is small), and also that the interface barriers I are perfectly smooth and have finite height $V(x)=V_0\delta(x)$ at $x=0$ and $x=a\equiv d_2$ and

$$\Delta(x)=\Delta[\theta(x-a)+\theta(-x)]+\Delta'\theta(a-x)\theta(x), \quad (2)$$

where Δ (Δ') is the magnitude of the order parameter in the S (S′) electrode. The effect of the electron-impurity scattering and of the imperfection of the interfaces we discuss later. Although such a model is not self-consistent,[20] in many cases it allows a simple analysis for the energy spectrum and for the electric current. A similar formulation was used in Ref. 23 to describe a hybrid superconductor/semiconductor device (so-called S/2DEG/S junction). However, the experimental S-I-S′-I-S setup used here, has properties being essentially distinct from those of the hybrid device,[23] because the middle electrode is a superconductor with nonzero order parameter and contributes to the Josephson coupling together with BS.

For the left-hand side S electrode of the S-I-S′-I-S stack we use the following trial wave function:

$$\kappa_l(x)=e^{i\varphi}(u_q e^{iq_+x}+a_q v_q e^{iq_-x}+b_q u_q e^{-iq_+x}), \quad (3a)$$

$$\nu_l(x)=e^{-i\varphi}(v_q e^{iq_+x}+a_q u_q e^{iq_-x}+b_q v_q e^{-iq_+x}). \quad (3b)$$

Here $u_q(v_q)$ is the coefficient of the Bogolubov transformation[21] and φ is the phase difference between the external and middle electrodes. The corresponding wave function for the right-hand side S electrode is a combination of incident and transmitted waves:

$$\kappa_r(x)=e^{-i\varphi}(c_q u_q e^{iq_+x}+d_q v_q e^{-iq_-x}), \quad (4a)$$

$$\nu_r(x)=e^{i\varphi}(c_q v_q e^{iq_+x}+d_q u_q e^{-iq_-x}). \quad (4b)$$

In the experiment, the values of the ratios Δ/ϵ_F and Δ'/ϵ_F are quite small, $\sim 10^{-3}$, which is typical for metals. Additionally, the potential barriers at the interface are very sharp and thin, with the thickness being of order $(1-10)k_F^{-1}$. It means that in the electrodes one can use the quasiclassical approximation, assuming that the electron (hole) momentum is $q_\pm=k_F\pm q_s$, k_F is the Fermi momentum, and q_s is the superfluid momentum [in the calculations, the momentum is normalized by Planck constant, $\hbar$; the length is expressed in units of $\hbar v_F/\Delta$, a value which is comparable with the BCS coherence length in the ''clean'' limit, $\xi=\hbar v_F/(\pi\Delta)$]. It also allows us to describe the influence of the interfaces using appropriate boundary conditions.

In the middle S′ electrode one also has

$$\kappa_m(x)=a_m v'_q e^{iq'_-x}+d_m v'_q e^{-iq'_-x}+b_m u'_q e^{iq'_+x}+c_m u'_q e^{-iq'_+x}, \quad (5a)$$

$$\nu_m(x)=a_m u'_q e^{iq'_-x}+d_m u'_q e^{-iq'_-x}+b_m v'_q e^{iq'_+x}+c_m v'_q e^{-iq'_+x}, \quad (5b)$$

that describes the electrons and holes traveling in the S′ region and where $q'_\pm$ is the electron (hole) momentum in that region. The above trial function does not include multiple Andreev scattering[2] because of the finite barriers at the interfaces.

The boundary conditions at the interface $x=0$ can be written as

$$\kappa_l(x)|_{x=-0}=\kappa_m(x)|_{x=+0}, \quad (6a)$$

$$\nu_l(x)|_{x=-0}=\nu_m(x)|_{x=+0}, \quad (6b)$$

$$\left.\frac{\partial\kappa_l(x)}{\partial x}\right|_{x=-0}-\left.\frac{\partial\kappa_m(x)}{\partial x}\right|_{x=+0}=k_F Z\kappa_m(x)|_{x=+0}, \quad (6c)$$

$$\left.\frac{\partial\nu_l(x)}{\partial x}\right|_{x=-0}-\left.\frac{\partial\nu_m(x)}{\partial x}\right|_{x=+0}=k_F Z\nu_m(x)|_{x=+0}, \quad (6d)$$

where $Z=V_0/E_F$ is the interface barrier strength, V_0 is the barrier height, and E_F is the Fermi energy. Combination with the similar boundary conditions at $x=a$ provides the set of linear equations for the coefficients.

In our approximation, for the coefficients of the Bogolubov transformation entering the above formulas (3), (4), and (5), one can use

$$u_E^2=1-v_E^2=\frac{1}{2}\left(1+\frac{\sqrt{E^2-\Delta^2}}{E}\right) \quad (7)$$

and $q_s(E)=\sqrt{E^2-\Delta^2}/v_F$, where v_F is the Fermi velocity. Similar formulas for $u'_E(v'_E)$ are obtained by replacing Δ by Δ' in Eq. (7). The excitation spectrum, $E_n(\varphi)$, may be found from the condition $\det[\hat{M}]=0$, where $\hat{M}$ is the matrix (8×8). In this way, for the BS energy in the limiting case $a\to 0$ (the S-I-S junction), one finds (see Refs. 7–9):

$$E(\varphi)=\pm\frac{\Delta}{\sqrt{2}}\sqrt{\frac{1+2Z^2+\cos\varphi}{1+Z^2}}, \quad (8)$$

For the simplest case, e.g., of the mesoscopic SIS junction with only one electron degree of freedom, at zero temperature, the Josephson current is

$$I(\varphi)=\frac{2\pi}{\Phi_0}\sum_n\frac{\partial E_n(\varphi)}{\partial\varphi}=\sqrt{2}\frac{\pi\Delta}{eR_0}\frac{\sin\varphi}{\sqrt{(1+Z^2)(1+2Z^2+\cos\varphi)}}, \quad (9)$$

where $R_0^{-1}=2e^2/h$ is the quantum conductance. If there is a degeneracy of the electron states (e.g., over the angle between the incident electron momentum **p** and the normal vector to the junction's interface **n**), then R_0^{-1}

$=N_{\rm eff}(2e^2/h)$, where $N_{\rm eff}$ is the effective degree of degeneracy. In that case, one obtains for the normal-state resistance of the junction an expression:

$$\frac{1}{R_{\rm N}}=\frac{1}{R_0}\frac{1}{1+Z^2}. \tag{10}$$

Alternatively, the expression for the junction resistivity may be obtained calculating the NIN geometry. If one expresses it via the electron reflection coefficient b, it gives the same result:

$$\frac{1}{R_{\rm N}}=\frac{1}{R_0}(1-|b|^2)=\frac{1}{R_0}\frac{1}{1+Z^2}. \tag{11}$$

In terms of the Blonder-Tinkham-Klapwijk[24] approach, $N_{\rm eff}=hN(0)v_{\rm F}\mathcal{A}$ providing that

$$\frac{1}{R_{\rm N}}=\frac{2N(0)e^2v_{\rm F}\mathcal{A}}{1+Z^2},$$

where $N(0)$ is the electron states density at the Fermi level, $\mathcal{A}$ is the effective area of the junction. For $Z\to 0$, Eq. (9) describes the Josephson current across a barrierless (ballistic) S-c-S point contact.[25] As Z grows, the dependence becomes proportional to $\sin\varphi$, like that for the tunnel junction.

For the S-I-S′-I-S junction with δ-function barriers at the interfaces, the explicit expression for the Josephson current is not available and only the numerical procedure provides the results. However, above $T_{\rm c}$, for the normal-state NININ junction, one can obtain the electron reflection coefficient as

$$B=|b|^2=\left\langle\left|\frac{Z(-i-Z+e^{2\,iak_{\rm F}}Z-ie^{2\,iak_{\rm F}})}{1-2\,iZ-Z^2+Z^2e^{2\,iak_{\rm F}}}\right|^2\right\rangle_{\rm osc}, \tag{12}$$

where a is the thickness of the middle layer, $k_{\rm F}$ is the Fermi momentum. In Eq. (12), $\langle\ldots\rangle_{\rm osc}$ means that $|b|^2$ must be averaged over the fast oscillating factor $e^{2\,iak_{\rm F}}$. Then the resulting $R_{\rm N}^{-1}(Z)$ is slightly steeper compared to the case of NIN geometry. Since in the case $a\neq 0$ and $Z\neq 0$, explicit expressions for $E_n(\varphi)$ are also not available, the energy eigenvalues should be found numerically from the condition $D(E,\varphi)=\det(\hat{M})=0$, where $\hat{M}$ is the matrix 8×8.

The most spectacular contour plots of $D(E,\varphi)$ that determine the curves $E_n(\varphi)$, were found for relatively small Z. The dependences $D(E,\varphi)$ are shown in Figs. 3(a)–3(c) and Figs. 3(d)–3(f) for the fixed values $a=0.1$ and $a=3.1$, respectively, and various barrier strengths Z. In the plots, the bound states energy $E_n(\varphi)$ is expressed in units of the energy gap Δ at $T=0$ while the phase difference φ is measured in radians. The calculations were carried out using $\Delta'=0.3$ and the value of the inelastic scattering rate $\Gamma\simeq{\rm Im}\,\Delta=0.15$. Comparing Figs. 3(a)–3(c) and 3(d)–3(f), one finds a tendency that the shape of the energy levels of the BS undergoes topological transformations as Z is varied. In addition, the shape of the bound state levels is quite different for the limits $a\ll\xi$ [Figs. 3(a)–3(c)] and $a\gg\xi$ [Figs. 3(d)–3(f)] limits. Contrary to the simplest case of $a\to 0$, where only one bound state (with $E_n>0$) is present and

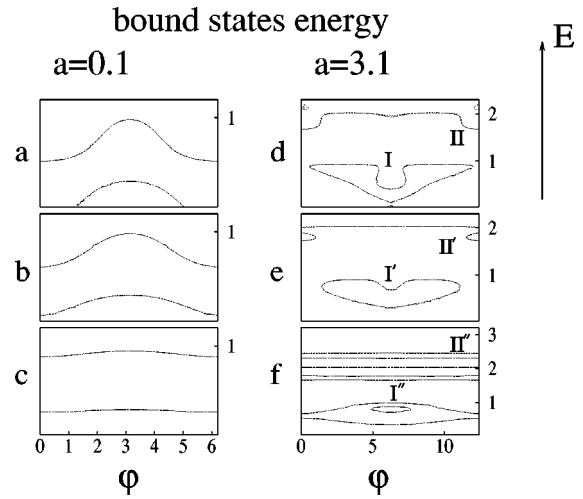

FIG. 3. The contour plots for the bound states in the S-I-S′-I-S device for different thicknesses a of the middle electrode and various interface barrier height Z: (a, d) $Z=0.03$; (b, e)$Z=1.5$; (c) $Z=3.5$; (f) $Z=2.5$. The phase is measured in radians, the energy is measured in units of Δ at $T=0$.

where the energy $E_n(\varphi)$ oscillates versus φ, the shape of the BS for finite a can become closed between some values of the phase difference $\varphi_{1,2}$, forming localized ''islands'' [e.g., see Fig. 3(a)]. At $Z=0.03$ in Fig. 3(a), one can see a localized ''island'' positioned between $\varphi_1\approx\pi/2$ and $\varphi_2\approx 3\pi/2$. There is also another unlocked level positioned at higher energies that oscillates with φ. Thus the spectrum that is formed under the condition of Andreev reflection may have a complicated structure, and in analogy with classical mechanics can be viewed as a combination of ''continuous'' and ''finite''motion. As the barrier height increases to $Z=1.5$ [see Fig. 3(b)], the ''island'' becomes unlocked, and both the BS oscillate with φ. At $Z\geqslant 3.5$, $E_n(\varphi)$ becomes smoothly oscillating [e.g., see Fig. 3(c)].

The ''island'' BS and oscillating BS are combined at some values of a. This situation is shown in Fig. 3(d) plotted for $a=3.1$ and small $Z=0.03$. Again, one may observe a big ''island'' at low energies $E<\Delta$ (marked as I), in addition to an unlocked scattering state at high energies [curve II in Fig. 3(d)] which, however, has sharp bends at $\varphi_1\approx\pi/2$ and $\varphi_2\approx 7\pi/2$. As the barrier strength increases, the shape of the $E_n(\varphi)$ curves gradually changes [see Fig. 3(e) plotted for $Z=1.5$]. The ''island'' BS becomes rounded [see curve I′ in Fig. 3(e)], while the scattering state [the former curve II in Fig. 3(d)] splits into a smooth scattering state and two additional ''islands'' [which are shown in Fig. 3(e) as curve II′]. The topological transformations continue as the barrier strength increases up to $Z=2.5$ [see Fig. 3(f)]. The ''island'' I′ from the previous figure [Fig. 3(e)] splits into the two oscillating continuous BS with a small additional ''island'' positioned between them (see curves I″), while the other small ''islands'' II′ transform into the set of scattering states II″.

The cause of the aforementioned topological transformation of $E_n(\varphi)$ is related to a complex interference between electrons and holes in Andreev reflection processes (ARP) in the S-I-S′-I-S structures with finite Z. The interface barriers modify the probability of ARP resulting in additional BS

levels, although not all of them are ''permitted'' at finite φ. When at some φ_i no levels are permitted, the trajectory becomes locked. This situation corresponds to a classic finite motion of a particle between two coordinates φ_1 and φ_2, while for the system under consideration that is related to a localized state. The implicit influence of the interface barriers on ARP is the main reason why BS are topologically transformed. On the contrary, the direct contribution of normal reflection to resonances is not significant because the normal electron wavelength, $\lambda_N \sim 1/k_F$, is small. On the other hand, the much longer wavelength, $\lambda_Q \sim 1/q_s \approx a$ ($q_s \simeq \pi\Delta/\hbar v_F \ll k_F$ for a BCS superconductor), is involved in the resonant process.

The above idealized description is not generally valid, either if the concentration of impurities in the electrodes is high, or if the interface is not perfectly smooth. However, one can modify this approach to the cases (i) when the impurity concentration is not very high ($E_F\tau_i \gg 1$, τ_i is the electron-impurity scattering time), or (ii) when the electron scattering at the interfaces is not specular. The limit (i) is considered if in the above formulas (3)–(6), one replaces formally $E \to E[1 + i/(2\tau_i\sqrt{E^2-\Delta^2})]$ and $\Delta \to \Delta[1 + i/(2\tau_i\sqrt{E^2-\Delta^2})]$. Then the modified E and Δ are used to perform the calculations of the $E_n(\varphi)$ curves in the same way as is described above. When the impurity concentration is increased, we have found that the curves $E_n(\varphi)$ become smoother, and the subtle details like those shown in Figs. 3(d)–3(f) are washed out. This is due to the finite width of the $E_n(\varphi)$ levels that itself depends on the magnitude of $E_F\tau_i$. The similar tendency is obtained also when the electron scattering at the S/S′ and S′/S interfaces becomes diffusive.

In the case (ii), the interface can be modeled by a mosaic structure that consists of N randomly inclined small elements M_i ($i = 1, \ldots, N$, the size of each element however must be larger compared to k_F^{-1}). Each element of the mosaic is characterized by its own area A_i and by its own normal vector $\mathbf{b}_i$, tilted in respect to the x-axis direction. Although the deviation of the normal vectors $\mathbf{b}_i$ is random, the condition $(1/N)\Sigma_i \mathbf{b}_i = \mathbf{b}$ ($\mathbf{b}$ is the vector along the x axis) has to be fulfilled. In such a setup, there are two major characteristics of the interface being important for the electron scattering. One is the tilting of the normal vectors $\mathbf{b}_i$ with respect to $\mathbf{b}$, that may be described by a distribution function $W_i(\theta_i, \phi_i)$ (where θ_i and ϕ_i are the tilting angles of $\mathbf{b}_i$). Another characteristic is the transmission diagram of the elementary electron tunneling process $\beta_i(\theta)$ (θ is the angle between the momentum of incident electron, $\mathbf{p}_{in}$, and $\mathbf{b}_i$) through the interface.[22] The electron scattering is considered separately for each element of the mosaic, and the set of $E_n^{(i)}(\varphi)$ is calculated, for different directions of $\mathbf{p}_{in}$. Then, the averaging over all the mosaic elements is made. Here we assume that all M_i have equal area, and the same transmission $\beta_i(\theta) = \beta(\theta) = \beta_0 \exp[-\theta^2/\gamma_{tr}]$ (β_0 is the normalizing constant, γ_{tr} is the dispersion over the angle of the elementary electron tunneling process). Also we use $W_i(\theta_i, \phi_i) = \exp[-\theta_i^2/\gamma_{tilt,1} - \phi_i^2/\gamma_{tilt,2}]$ with a dispersion $\gamma_{tilt,1} = \gamma_{tr}$ and $\gamma_{tilt,2} = \gamma_{tr}$. The finite result is similar to (i), but depends on the dispersion constant γ_{tr}. The general tendency is that the width of the $E_n(\varphi)$ levels is increased as γ_{tr} grows. This kind of behavior is consistent with the electron-impurity scattering effect. However, one can find that the width of the $E_n(\varphi)$ levels has a minor influence on the magnitude of the Josephson current, unless the topology remains unchanged (i.e., in the limit $E_F\tau_i \gg 1$, $\gamma_{tr} \ll \sqrt{\pi/2}$). When the parameters $E_F\tau_i$ and γ_{tr} increase, the topology of $E_n(\varphi)$ can eventually change, and the Josephson current then is affected as well. It should be noted that for a mosaic structure with tilted elements, the interface resistance is increased as compared with that for the ideally flat surface, and consequently, the N_{eff} and J_c are reduced. However, the detailed investigation of this problem is beyond the scope of this paper.

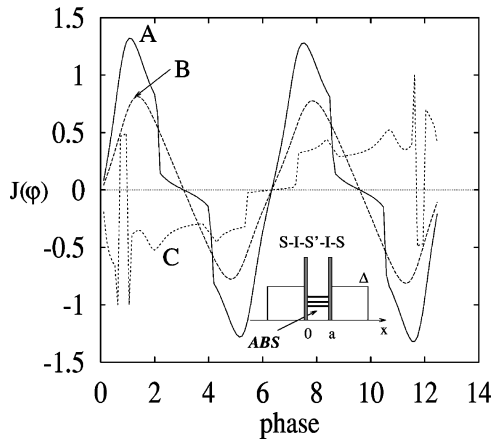

FIG. 4. The Josephson current versus phase difference in resonant conditions. Curves A, B, and C correspond to the band configurations shown in Fig. 3(a), 3(b), 3(d), respectively. The Josephson current is normalized by its maximum value, the phase is measured in radians. The Andreev band structure (ABS) for the S-I-S′-I-S configuration is schematically shown in the inset.

In Fig. 4 we have plotted the Josephson current versus the phase difference across the junction. In the inset to this figure we sketch the S-I-S′-I-S setup where we indicate that Andreev bound states (ABS) are positioned in the middle S′ electrode. The currents in Fig. 4 are measured in units of the critical current I_c of an ideal symmetric S-c-S point contact (with $Z = 0$) which has critical parameters being always higher compared to a nonsymmetric junction S-I-S′ ($Z \neq 0$; $\Delta' < \Delta$). From the curve A in this figure [which corresponds to the configuration of BS shown in Fig. 3(a) at $a = 0.1$ and $Z = 0.03$], one can see that the critical current, I_c, of the S-I-S′-I-S stack may be increased compared even to the barrierless S-c-S case (with $I_c = 1$ in our units), while the difference between S-I-S′-I-S and nonsymmetric S-I-S′ junctions must be even more significant. One may also notice a deviation from the regular sin φ dependence due to presence of the bends at $\varphi_1 \simeq \pi/2$ and $\varphi_2 \simeq 3\pi/2$. Referring to Fig. 3(a), one can conclude that the bends originate from the ''island'' BS closed between φ_1 and φ_2. These bends are hampered in curve B for which the barrier strength increases up to $Z = 1.5$ [this case corresponds to BS shown in Fig. 3(b)], thus the shape of the Josephson characteristic transforms to a shape like that for a regular tunnel junction, $I(\varphi) = I_c \sin\varphi$ (e.g., see curve B in Fig. 4). Interesting $I(\varphi)$ characteristics correspond to the case $a > \xi$ with BS shown in Figs. 3(d)–3(f). In that case, the complex topology of BS and of scattering states, consisting of closed ''islands,'' results in a

quite remarkable $I(\varphi)$ dependence, as well. More specifically, the ''islands'' lead to irregular alternation of the Josephson current at some values of the phase difference. This kind of characteristic is shown as curve C in Fig. 4, which corresponds to the $E_n(\varphi)$ contours of Fig. 3(d). For example, the sharp edge of ''island'' II at $\varphi \simeq \pi/4$ [see Fig. 3(d)] produces the sudden cusp in the $I(\varphi)$ characteristics (see Fig. 4, curve C) at the same value of φ.

We have considered in detail the properties of the system with $Z<1$ and $Z\sim 1$, since this is the physically most spectacular case, which reveals the correlation between the electron spectrum and I_c in an obvious way. As the interface barrier strength Z grows, the $E_n(\varphi)$ contours become smoother, and the number of the BS contributing to $I(\varphi)$ increases. But even in the low-transparency limit, when $Z \gg 1$ (which is valid for commonly available tunnel junctions, including those used in our experiment), the critical current of the symmetric S-I-S′-I-S devices, in principle, always exceeds the value of I_c for the S-I-S′ junction due to a contribution of BS.

According to formula (1), there is another factor that may, in principle, affect the magnitude of I_c. For instance, if the electron distribution function f_{E_n} deviates from the equilibrium, the Josephson tunneling may be influenced. One may argue that, in the case of the Nb/Al-AlO_x-Nb/Al-AlO_x-Ta/Nb devices, we measure the critical current of the bottom Nb/Al-AlO_x-Nb/Al junction when the upper Nb/Al-AlO_x-Ta/Nb junction is in the resistive state at gap sum voltage. Therefore, the upper junction may be a source of the nonequilibrium influence in the following two ways. First, the extraction of quasiparticles is possible from the middle Nb/Al layer, which results in the stimulation of superconductivity.[26] However, in this case we would observe an increase, rather than a decrease, of the critical current through the bottom junction as compared with the critical current value measured on the Nb/Al-AlO_x-Nb/Al-AlO_x-Nb devices in equilibrium conditions ($V=0$). On the other hand, one may suppose that the energy gap in the middle electrode is suppressed by excess quasiparticles produced by pair breaking when the upper junction is biased at gap sum voltage. Then the critical current in the bottom junction may be suppressed, too. The same effect, if not stronger, should be observed on symmetric Nb/Al-AlO_x-Nb/Al-AlO_x-Nb devices with nearly identical critical currents, if one of the junctions is in the resistive state. Using proper biasing of two-terminal devices and measurements on three-terminal devices,[27] we observed the branches in the *I-V* characteristic displaying critical currents of both junctions from the stack (i.e., initial switching of one junction to single gap sum voltage and consequent switching of the second junction to the double gap sum voltage). We have found that the difference between the critical currents of the two junctions was much less than that discussed in this paper. Hence, for the kind of junctions we are working with, the nonequilibrium effects have only a minor influence on the Josephson critical current.

IV. CONCLUSION

From the above analysis one can conclude that the S-I-S′-I-S devices considered here reveal physical properties that have not been taken into account in the theories confined to inductive coupling between the junctions. In the model we have assumed that the middle S′ layer in the device is a superconductor with reduced superconducting parameters as compared with those for external electrodes. However, the same approach may be applied to the case when the middle electrode is a normal metal. In both cases, there is an ''energy quantum well'' formed by the superconducting energy gap profile of the successive electrodes. In such devices, the current-phase ratio may be substantially modified due to resonances that arise in the middle layer as a result of Andreev reflection. In particular, this may result in an enhancement of the supercurrent through the device. This effect was observed experimentally on Nb-based devices. Probably, the same approach may be used to explain the appearance of the supercurrent in Nb-AlO_x-Al-AlO_x-Nb devices.[28] It is important that such resonances be efficient even for devices with low transmission probability of the tunnel barriers and a middle electrode with good metallic properties, so that the normal electron wavelength is small. Due to the last fact, it is difficult to observe resonant tunneling of normal electrons through the double-barrier junctions with the middle electrode being metal. Therefore, resonant tunneling phenomena of normal electrons are usually restricted to semiconductor devices. However, even for metals, the resonance may be observable for a quasiparticle wave with the wavelength $\lambda_Q \sim 1/q_s$, which characterizes quasiparticles involved in Andreev reflection processes, because this wavelength is typically much larger than the wavelength of normal electrons. The value of λ_Q is comparable with the BCS coherence length, which reflects the fact that the excited quasiparticles bear the collective mode behavior of paired electrons. In this respect, the phenomenon is closely related to that described in Refs. 29,30.

ACKNOWLEDGMENTS

I. P. Nevirkovets was supported by the Royal Society (UK). The samples were fabricated and measured at the Department of Materials Science and Metallurgy (University of Cambridge, UK). This work was supported in part by the Northwestern Materials Research Center under NSF Grant No. DMR-9309061.

*Permanent address: Institute for Metal Physics, National Academy of Sciences of the Ukraine, 36 Vernadsky Boulevard, UA-252680 Kyïv-142, Ukraine.

†Permanent address: Institute of Magnetism, National Academy of Sciences of the Ukraine, 36b Vernadsky Boulevard, UA-252680 Kyïv-142, Ukraine.

[1] A. F. Andreev, Zh. Eksp. Teor. Fiz. **49**, 655 (1965) [Sov. Phys. JETP **22**, 455 (1966)].

[2] M. Octavio, M. Tinkham, G. E. Blonder, and T. M. Klapwijk, Phys. Rev. B **27**, 6739 (1983).

[3] A. D. Zaikin, Zh. Eksp. Teor. Fiz. **84**, 1560 (1983) [Sov. Phys. JETP **57(4)**, 910 (1983)].

[4] U. Gunsenheimer and A. D. Zaikin, Phys. Rev. B **50**, 6317 (1994).
[5] C. Ishii, Prog. Theor. Phys. **44**, 1525 (1970).
[6] A. V. Svidzinsky, T. N. Antsygina, and E. N. Bratus', Zh. Eksp. Teor. Fiz. **61**, 1612 (1971) [Sov. Phys. JETP **34**, 860 (1972)].
[7] S. V. Kuplevakhsikii and I. I. Fal'ko, Fiz. Nizk. Temp. **17**, 961 (1991) [Sov. J. Low Temp. Phys. **17**, 501 (1991)].
[8] C. W. J. Beenakker and H. van Houten, Phys. Rev. Lett. **66**, 3056 (1991).
[9] L.-F. Chang and P. F. Bagwell, Phys. Rev. B **49**, 15 853 (1994).
[10] K. Böttcher and T. Kopp, Phys. Rev. B **55**, 11 670 (1997).
[11] C. J. Lambert and R. Raimondi, J. Phys.: Condens. Matter **10**, 901 (1998).
[12] A. Barone and G. Paterno, *Physics and Application of the Josephson Effect* (Wiley, New York, 1982).
[13] K. K. Likharev, *Dynamics of Josephson Junctions and Circuits* (Gordon & Breach, New York, 1986).
[14] S. Kashiwaya, Y. Tanaka, M. Koyanagi, and K. Kajimura, Phys. Rev. B **53**, 2667 (1996).
[15] R. Kleiner, F. Steinmeyer, G. Kunkel, and P. Müller, Phys. Rev. Lett. **68**, 2394 (1992).
[16] S. Sakai, P. Bodin, and N. F. Pedersen, J. Appl. Phys. **73**, 2411 (1993).
[17] S. Sakai, A. V. Ustinov, H. Kohlstedt, A. Petraglia, and N. F. Pedersen, Phys. Rev. B **50**, 12 905 (1994).
[18] I. P. Nevirkovets, J. E. Evettes, M. G. Blamire, Z. H. Barber, and E. Goldobin, Phys. Lett. A **232**, 299 (1997).
[19] I. P. Nevirkovets, M. G. Blamire, and J. E. Evetts (unpublished).
[20] A. B. Svidzinskiy, *Space-inhomogeneous Issues of the Superconductivity Theory* (Science, Moscow, 1982, in Russian), p. 310.
[21] P. G. de Gennes, *Superconductivity of Metals and Alloys* (Benjamin, New York, 1966).
[22] S. E. Shafranjuk and T. Yamashita, Phys. Rev. B **54**, 15 380 (1996).
[23] A. Chrestin, T. Matsuyama, and U. Merkt, Phys. Rev. B **49**, 498 (1994).
[24] G. E. Blonder, M. Tinkham, and T. M. Klapwijk, Phys. Rev. B **25**, 4515 (1982).
[25] I. O. Kulik and A. N. Omel'yanchuk, Fiz. Nizk. Temp. **3**, 945 (1977) [Sov. J. Low Temp. Phys. **3**, 459 (1977)]; **4**, 296 (1978) [**4**, 142 (1978)].
[26] M. G. Blamire, E. C. G. Kirk, J. E. Evetts, and T. M. Klapwijk, Phys. Rev. Lett. **66**, 220 (1991).
[27] I. P. Nevirkovets, J. E. Evetts, and M. G. Blamire, Phys. Lett. A **187**, 119 (1994).
[28] M. Maezawa and A. Shoji, Appl. Phys. Lett. **70**, 3603 (1997).
[29] W. J. Tomash, Phys. Rev. Lett. **15**, 672 (1965).
[30] W. L. McMillan and P. W. Anderson, Phys. Rev. Lett. **16**, 453 (1966).